THE ASTROPHYSICAL JOURNAL, 461:408–414, 1996 April 10
© 1996. The American Astronomical Society. All rights reserved. Printed in U.S.A.

1996ApJ...461..408A

THE COSMIC-RAY ENERGY SPECTRUM BETWEEN $10^{14.5}$ AND $10^{16.3}$ eV COVERING THE "KNEE" REGION

M. AMENOMORI,[1] Z. CAO,[2] B. Z. DAI,[3] L. K. DING,[2] Y. X. FENG,[3] Z. Y. FENG,[4] K. HIBINO,[5] N. HOTTA,[6] Q. HUANG,[4] A. X. HUO,[2] H. Y. JIA,[4] G. Z. JIANG,[4] S. Q. JIAO,[4] F. KAJINO,[7] K. KASAHARA,[5] LABACIREN,[8] S. M. LIU,[2] D. M. MEI,[8] L. MENG,[2] X. R. MENG,[8] MIMACIREN,[8] K. MIZUTANI,[9] J. MU,[3] H. NANJO,[1] M. NISHIZAWA,[10] M. OHNISHI,[10] I. OHTA,[6] T. OUCHI,[10] J. R. REN,[2] TO. SAITO,[11] M. SAKATA,[7] Z. Z. SHI,[2] M. SHIBATA,[12] A. SHIOMI,[9] T. SHIRAI,[5] H. SUGIMOTO,[13] X. X. SUN,[2] K. TAIRA,[13] Y. H. TAN,[2] N. TATEYAMA,[5] S. TORII,[5] H. WANG,[2] C. Z. WEN,[4] Y. YAMAMOTO,[7] G. C. YU,[4] P. YUAN,[2] T. YUDA,[10] C. S. ZHANG,[2,10] H. M. ZHANG,[2] L. ZHANG,[3] ZHASANG,[8] ZHAXICIREN,[8] AND W. D. ZHOU[3]
(The Tibet ASγ Collaboration)

Received 1995 June 2; accepted 1995 October 13

ABSTRACT

The Tibet array is the first air shower detector to search for 10 TeV gamma-ray point sources. This array also has a high sensitivity to air showers initiated by cosmic rays around the "knee" of the all-particle spectrum at 10^{15}–10^{16} eV, with quite small ambiguity for the energy estimation, since the development of air showers in this high energy region is close to maximum at Yangbajing altitude (4300 m above sea level).

Using the data set taken with the Tibet array in the period from 1990 October through 1993 July, we obtained the differential energy spectrum of primary cosmic rays between 3×10^{14} and 2×10^{16} eV covering the knee region. The overall spectrum obtained does not resemble a single power law and shows a gradual steepening of the slope at energies around $10^{15.25}$ eV.

The spectrum is expressed as

$$J(E_0) = 1.5 \times 10^{-20}(E_0/10^{14.75}\ \text{eV})^{-2.60\pm0.04}(\text{m}^{-2}\ \text{s}^{-1}\ \text{sr}^{-1}\ \text{eV}^{-1}) \text{ at } E_0 < 10^{14.75}\ \text{eV}$$

and

$$J(E_0) = 1.2 \times 10^{-23}(E_0/10^{15.85}\ \text{eV})^{-3.00\pm0.05}(\text{m}^{-2}\ \text{s}^{-1}\ \text{sr}^{-1}\ \text{eV}^{-1}) \text{ at } E_0 > 10^{15.85}\ \text{eV},$$

where this changes gradually between $10^{14.75}$ and $10^{15.85}$ eV and takes the value $J(E_0) = 6.7 \times 10^{-22}$ ($\text{m}^{-2}\ \text{s}^{-1}\ \text{sr}^{-1}\ \text{eV}^{-1}$) at $E_0 = 10^{15.25}$ eV.

Subject headings: cosmic rays

1. INTRODUCTION

The energy range between 10^{14} and 10^{16} eV has been the subject of particular interest. A major feature in the observed spectrum occurs around the so-called knee between 10^{15} and 10^{16} eV, where the slope of the all-particle energy spectrum seems to change rather abruptly. An attractive possibility is that such a steepening is a consequence of the breakdown of an acceleration mechanism at high energy. At present, the most promising theory for the source of the bulk of the cosmic rays is shock acceleration of particles in supernova blast waves. There is, however, general agreement that cosmic-ray acceleration at supernova remnants (SNRs) appears to have a natural upper limit of about $Z \times 10^{14}$ eV (Lagage & Cesarsky 1983), which depends upon the rate at which the particles can gain energy and the lifetime of the shock. Of course, one can probably extend this value somewhat by involving multiple supernovae (see, e.g., Axford 1991, 1994) and magnetic field effects (Jones & Ellison 1991; Naito & Takahara 1995), but it is unlikely that particle energies much higher than 10^{15} eV can be achieved. Cosmic-ray acceleration at SNRs would also suggest that elemental composition changes dramatically at energies around the knee energy region; that is, the knee should be filled in by nuclei with higher charge Z. The energy spectrum above 10^{16} eV is significantly steeper than that measured below, but the spectrum extends to much higher energies, say $\sim 10^{20}$ eV (Bird et al. 1994; Yoshida et al. 1995). So other acceleration mechanisms will be active in the highest energy region (see, e.g., Hillas 1984; Protheroe & Szabo 1992), and the very highest energy cosmic rays ($>10^{19}$ eV) may be of extragalactic origin. On the other hand, there is an alternative explanation that the break of the spectrum around the knee represents the energy at which cosmic rays can escape more freely from the trapping zone in the Galactic disk (Peters 1959; Hillas 1981). If the steepening depends on rigidity in the same way for all nuclei, then the relative fraction of heavy nuclei is expected to increase with primary energy. It

[1] Department of Physics, Hirosaki University, Hirosaki 036, Japan.
[2] Institute of High Energy Physics, Academia Sinica, Beijing 100039, China.
[3] Department of Physics, Yunnan University, Kunming 650091, China.
[4] Department of Physics, South West Jiaotong University, Chengdu 610031, China.
[5] Faculty of Engineering, Kanagawa University, Yokohama 221, Japan.
[6] Faculty of Education, Utsunomiya University, Utsunomiya 321, Japan.
[7] Department of Physics, Konan University, Kobe 658, Japan.
[8] Department of Mathematics and Physics, Tibet University, Lhasa 850000, China.
[9] Department of Physics, Saitama University, Urawa 338, Japan.
[10] Institute for Cosmic Ray Research, University of Tokyo, Tanashi 188, Japan.
[11] Tokyo Metropolitan College of Aeronautical Engineering, Tokyo 116, Japan.
[12] Faculty of Education, Yokohama National University, Yokohama 240, Japan.
[13] Shonan Institute of Technology, Fujisawa 251, Japan.

© American Astronomical Society • Provided by the NASA Astrophysics Data System

1996ApJ...461..408A

is, however, pointed out that the break appears to be rather too sharp for this scenario to work easily (Hillas 1984). A new component that dominates above 10^{14}–10^{15} eV might compensate for this deficiency (Fitchel & Linsley 1986; Protheroe & Szabo 1992).

In any case, the knee appears to mark a change in the acceleration and/or propagation mechanism for higher energy particles, and, accordingly, a knowledge of the precise shape of the spectrum as well as the composition around the knee energy region is crucial for discriminating among the possibilities.

To date, many measurements of the primary spectra have been done with various methods at energies around the knee. Direct measurements of the energy spectrum below 10^{14} eV have been reported by Grigorov et al. (1971) and the JACEE Collaboration (Burnett et al. 1993), while the Akeno group (Nagano et al. 1984) extensively studied the spectrum around the knee and beyond with air shower techniques. However, there is still some disagreement about the details around the knee (Lloyd-Evans 1992). The results obtained at Akeno (Nagano et al. 1984) seem to suggest a sharp break of the primary spectrum between 10^{15} and 10^{16} eV. It should be noted that air shower measurements at or near sea level have a serious bias in the detection of showers when their primary energies are less than $\sim 10^{16}$ eV, resulting in a strong dependence of the primary spectrum estimated from such observations on the primary-mass composition. In 1965, the BASJE group (Bradt et al. 1965) estimated the primary spectrum around the knee using air showers observed at Mount Chacaltaya (5200 m above sea level), where small air showers can be detected with very high efficiency. This result, however, is based on the longitudinal development curves obtained from constant-intensity cuts on the size spectrum plots measured at various zenith angles, and is thus dependent upon the primary-mass composition. There is, therefore, a need to establish the cosmic-ray spectrum around the knee based on a reliable observation.

A new generation of air shower experiments at high altitude designed primarily for ultra–high-energy gamma-ray astronomy should be very sensitive to showers induced by primaries with energies from 10^{14} to 10^{16} eV, covering the entire range in which the knee of the spectrum occurs. Among these, a Tibet air shower array has successfully operated at Yangbajing in Tibet (4300 m above sea level, 606 g cm^{-2}, 90°.53 E and 30°.11 N) since 1990 January. Using this array, we have searched for a steady emission of gamma rays around 10 TeV from the promising candidates of cosmic-ray sources (Amenomori et al. 1992, 1994). We have also studied the shadowing of cosmic rays by the Moon and the Sun (Amenomori et al. 1993a, b). This array is shown to have a high sensitivity to air showers initiated by cosmic rays with energies around the knee, since the Yangbajing altitude is near the maximum for such air shower developments in the atmosphere.

In this paper, we present the total energy spectrum of primary cosmic rays in the energy region involving the knee, using the data set obtained with this array.

2. EXPERIMENT

A schematic view of the Tibet air shower array is shown in Figure 1. The array consists of 65 plastic scintillation detectors placed on a lattice with 15 m spacing. A lead plate of 5 mm thickness is positioned on the top of each detector

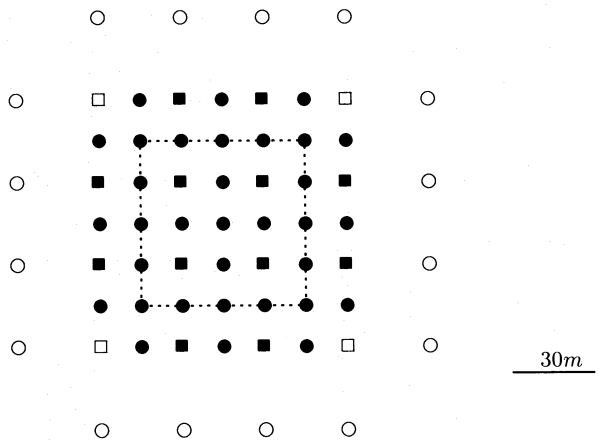

FIG. 1.—Schematic view of the Tibet AS array. For explanation of symbols and dotted lines see text.

to increase the number of shower particles by converting photons in the air shower into electron-positron pairs. The inner 45 FT (fast-timing) detectors of 0.5 m^2 each (*filled circles and filled squares*) are equipped with fast-response photomultipliers (PMs) with a transit-time spread of less than 0.55 ns. The signal of each detector is used to measure both particle density (with an analog-to-digital converter) and duration of the shower front (with a time-to-digital converter). Among these, furthermore, 12 FT detectors (*filled squares*) are equipped with wide dynamic range PMs to measure the particle densities near the core region of very high energy showers whose cores fall in the array. This FT array is surrounded by 20 density detectors (*open squares*, 0.5 m^2 each; *open circles*, 0.25 m^2 each) to obtain a good core location for each shower event.

This array has already been shown to be very powerful in detecting small air showers at energies around 10^{13} eV (Amenomori et al. 1992, 1994). In addition, it is also capable of detecting air showers at energies around 10^{14}–10^{17} eV with extremely high efficiency using the detectors equipped with wide dynamic range PMs in the array. These detectors (*filled and open squares*), placed on a lattice with 30 m spacing, as shown in Figure 1, are very helpful in observing the lateral distributions of ultra–high-energy air showers at energies around 10^{16} eV. The arrival direction of each air shower is accurately determined with a fast-timing method using 45 FT detectors. The overall angular resolutions of the array are estimated to be about 1° in the energy region around 10^{13} eV and 0°.5 at 10^{14} eV (Amenomori et al. 1993a).

In this analysis, we used the data set taken during the period from 1990 October through 1993 July. The data were taken from any fourfold coincidence in the 45 FT detectors, each of which was hit by more than 1.25 particles. The trigger frequency was about 20 Hz (40 Hz) at the time from 1990 October to 1992 September (from 1992 October to 1993 July). The dead time of the system is then estimated to be 9% and 15% for 20 Hz and 40 Hz data, respectively. The effective running time used for the present analysis is 6.16×10^7 s (713.5 days).

3. MONTE CARLO SIMULATION

Air showers, each being generated by a high-energy cosmic ray very high in the atmosphere, are the products of a large number of interactions successively occurring at

© American Astronomical Society • Provided by the NASA Astrophysics Data System

1996ApJ...461..408A

various atmospheric depths. These stochastic fluctuations, together with experimental bias, deform the observed air showers considerably, so a Monte Carlo simulation is indispensable in deriving reliable results from the experimental data.

An extensive Monte Carlo simulation of air showers to be observed at Yangbajing altitude was done using a GENAS code (Kasahara & Torii 1991). The detailed Monte Carlo simulation helps evaluate the detection efficiency and bias on the air showers observed with the Tibet array. In this simulation we carefully examined how the nature of primary cosmic rays affects the air shower developments in order to keep our results as free as possible from the primary mass composition, and also to eliminate some systematic detection bias.

3.1. *Features of Air Showers Observed at Yangbajing*

Our analysis aims to obtain the energy spectrum of primary cosmic rays from the air shower measurements in a way that depends as little as possible on uncertainties of the primary mass composition. In such an experiment, the primary energy of each event must be estimated from the (electron) size of the observed air shower, which fluctuates considerably from event to event even if the primary energy is the same. This size fluctuation is mostly caused by a large fluctuation of the starting depth of air shower development. It may, however, be shown that the shower size around the maximum air shower development, with a minimum fluctuation, is almost proportional to the primary energy.

Shown in Figure 2 are the longitudinal developments of the average air shower sizes in the atmosphere induced by proton (*crosses*) and iron (*open circles*) primaries for a vertical incidence. This figure explains well why the Tibet array is so suitable for our intended purpose; that is, (1) air showers induced by particles with energies $\sim 10^{14}$–10^{17} eV reached their maximum developments at Yangbajing altitude, thus their size fluctuations become a minimum, less than 20% for proton primaries and less than 10% for iron primaries, and (2) the average shower size becomes almost the same at Yangbajing altitude for both proton and iron primaries, if they are of the same primary energy, in the energy range between $\sim 10^{14}$ and 10^{17} eV. These facts ensure the ability to estimate the energy of primary particles with quite small ambiguity by measuring only their air shower sizes, almost independent of the primary composition.

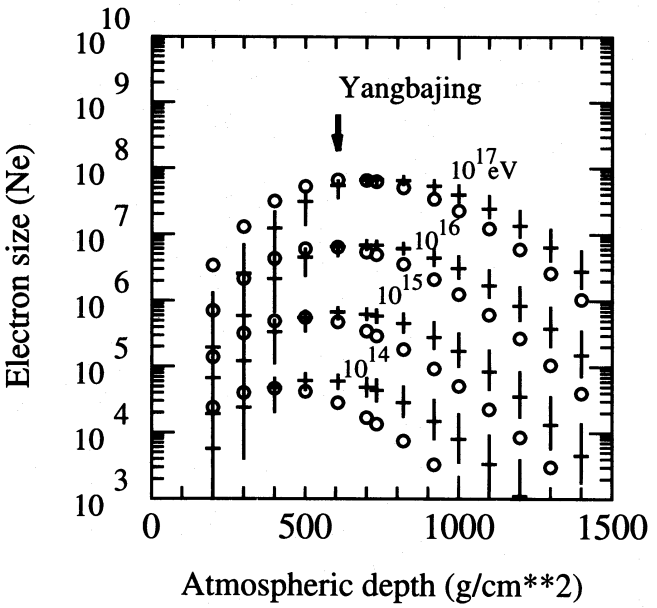

FIG. 2.—Average transition curves of air showers induced by protons (*crosses*) and iron nuclei (*open circles*) for a vertical incidence. The vertical bar of each cross denotes 1 standard deviation of the size distribution at the respective depth.

The determination of the lateral distribution function of shower particles is then substantially important in this experiment, since the total number of shower particles is estimated by fitting this to the experimental data. Using the Monte Carlo data obtained under the same conditions as the experiment, we found that the following function can be fitted well to the lateral distribution of shower particles under a lead plate of 5 mm thickness:

$$F(x, s) = Ne \frac{C_1(s)}{R_m^2} x^a(1 + x)^b(1 + cx^d) ,$$

$$C_1(s) = 2\pi[B(a + 2, -b - a - 2) + cB(a + d + 2, b - a - d - 2)]^{-1} ,$$

where $a = s - 2.2$, $b = s - 7.5$, $c = 2.5$, $d = 3.45 - s$, $x = r/R_m$, and $R_m = r_m \cos^{0.85} \theta$. The variable s corresponds to the *age parameter*, Ne is the total number of shower particles, r_m is the Molière unit (133 m at Yangbajing altitude), and $B(\alpha, \beta)$ is the beta function. This expression is valid in the range of $s = 0.6 \sim 1.6$, $\cos \theta = 0.6 \sim 1.0$ and $r = 10 \sim 300$ m. The air shower size is enhanced, on an average, by a factor of 2.1 under the lead plate of 5 mm thickness which is almost independent of the primary energy (Amenomori et al. 1990). In order to fix the values of the numerical parameters appearing in the function, we used the Monte Carlo results obtained by Kasahara, Yuda, & Torii (1990).

3.2. *Primary Spectra and Composition*

Air shower observation at Yangbajing covers a range of shower sizes from $\sim 10^5$ to 10^8 particles, corresponding roughly to the primary energies between 10^{14} and 10^{17} eV. Their interpretation depends on the assumption regarding the nature of the particles which initiate the showers. For example, for heavier nuclei, the showers start higher in the atmosphere and develop rapidly; so for a given primary energy there are fewer particles left at observation level. Thus, the energy estimates are generally affected by the assumed composition of primary cosmic rays. In order to obtain a reliable conclusion, we examined the effects of the nature of primary composition carefully. In this Monte Carlo simulation, four different models are examined for primary cosmic rays: (1) heavy dominant chemical composition (HD1); (2) proton dominant chemical composition (PD1); (3) pure proton (P); (4) pure iron (Fe). Among these, models 1 and 2 are critically examined. The shape of the all-particle spectrum is assumed to be the same for both cases. A major difference between these models is the ratio of the number of protons and iron nuclei to the total at higher energies (for details see Ren et al. 1988). At 10^{16} eV, for example, the fractions of protons and iron nuclei are 14% and 42% for the HD1 model and 28% and 15% for the PD1 model, respectively. Note that some recent experiments (Ren et al. 1988; Bird et al. 1993; Saito et al. 1993; Burnett et al. 1993 are in favor of model 1).

© American Astronomical Society • Provided by the NASA Astrophysics Data System

1996ApJ...461..408A

TABLE 1

SUMMARY OF MODELS EXAMINED IN THE MONTE CARLO SIMULATION[a]

Model	Primary Kind	Power ($<E_b$)	E_b (eV)	Power ($>E_b$)	Bend
HD1.....	P, He, L	2.7	$\langle Z\rangle \times 3 \times 10^{14}$	3.0	gradually
	MH, H, VH	2.6	$\langle Z\rangle \times 3 \times 10^{14}$	3.0	gradually
	Fe	2.5	$\langle Z\rangle \times 3 \times 10^{14}$	3.0	gradually
PD1	P, He, L	2.7	4.2×10^{15}	3.0	gradually
	MH, H, VH, Fe	2.6	4.2×10^{15}	3.0	gradually
P.....	P	2.65	4.2×10^{15}	3.0	abruptly
Fe	Fe	2.65	4.2×10^{15}	3.0	abruptly

[a] E_b stands for the bending energy of each component.

Other models (3 and 4) were also examined to obtain information about some limiting result. Details of these models are summarized in Table 1.

4. ANALYSIS

4.1. *Data Selection*

As discussed above, the air showers observed at Yangbajing with smaller zenith angles are almost independent of the nature of the primary particles when their primary energies are higher than $\sim 10^{14}$ eV. So we first selected the high-energy shower data from the original data set by imposing the following conditions:

1. Each of any 10 detectors, among the inside 49 detectors, should detect a signal of more than five particles.
2. The zenith angle (θ) of each air shower should be less than 25°, or sec $\theta \leq 1.1$.
3. The core position of each shower should be inside the innermost 5 × 5 detectors, or their coordinates: $|xw\alpha| \leq 30$ m, and $|yw\alpha| \leq 30$ m (corresponding to the square surrounded by the dotted line in Fig. 1), where the core position ($xw\alpha$, $yw\alpha$) is estimated by using the equations

$$xw\alpha \equiv \sum_{i=1}^{65} x_i \rho_i^\alpha \Big/ \sum_{i=1}^{65} \rho_i^\alpha , \quad yw\alpha \equiv \sum_{i=1}^{65} y_i \rho_i^\alpha \Big/ \sum_{i=1}^{65} \rho_i^\alpha$$

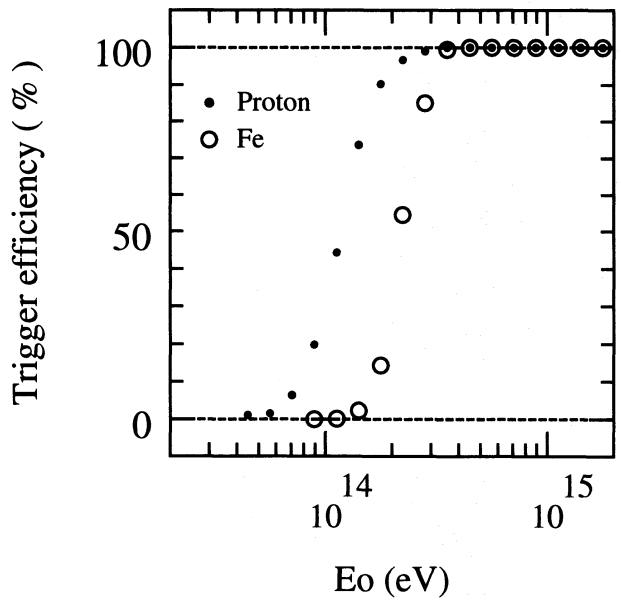

FIG. 3.—Trigger efficiencies of air showers induced by proton and iron primaries, respectively.

where ρ_i is the particle density at the ith detector and the weight parameter $\alpha = 8$. This large α-value is effective in locating the core position of low-energy showers quickly. For high-energy showers, however, a much smaller value is better; therefore, we calculate the estimation for these showers later.

The same selection was also made for the Monte Carlo simulation showers, where we checked the trigger efficiencies of showers induced by protons and iron nuclei in the atmosphere, as shown in Figure 3. The efficiencies for showers induced by other nuclei are distributed evenly between two cases. It is confirmed by these simulations that the air showers induced by primary particles with $E_0 \geq 400$ TeV and $\theta < 25°$ can be fully detected by the Tibet array without any bias.

Under these conditions, the effective detection area S of the Tibet array then becomes 3600 m^2 (its error is less than a few percent) for the vertical showers. This area of course becomes smaller for inclined showers. The total effective area $S \times \Omega$ is also calculated to be 1.96×10^3 m^2 sr for all primary particles with $E_0 \geq 300$ TeV. For the operation period from 1990 October through 1993 July, the effective running time T was 6.16×10^7 s. The total number of air showers selected under the above conditions is 2.60×10^6 events. These high-energy showers are studied further to obtain the energy spectrum of primary cosmic rays.

4.2. *Procedure to Estimate the Primary Spectrum*

In Figure 4 we show the scatter plots of the primary energy, E_0, and the air shower size under the lead plate, Ne(UL), those being selected under the conditions in the preceding section in the case of the HD1 model. It is seen that the width of the size distribution for a fixed primary energy decreases as the primary energy increases. For example, $\Delta Ne/Ne = 27\%$ at $E_0 = 4 \times 10^{14}$ eV, while it is 17% at 2×10^{15} eV (ΔNe denotes 1 standard deviation). A strong linear correlation between them seen in this figure is one of the advantages of observing air showers at high altitude.

Figure 5 shows the correlations between the average shower size under the lead plate, Ne(UL), and the primary energy E_0 for respective primary models. It is remarkable and important that there is no substantial difference between models PD1 and HD1 in the energy region of interest. Minute differences seen between them of course become larger as the zenith angle of observed showers increases, suggesting an increasing dependence of air shower size on the primary composition at lower altitude. As seen in this figure, however, the proton and iron primary

© American Astronomical Society • Provided by the NASA Astrophysics Data System

1996ApJ...461..408A

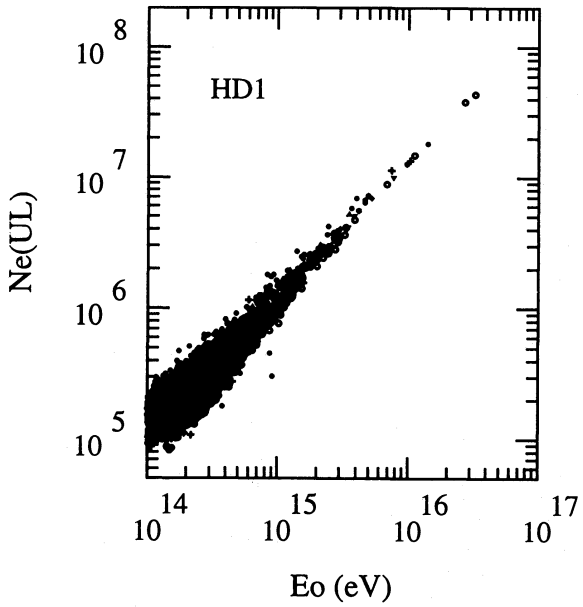

FIG. 4.—Scatter plots of the primary energy E_0 and the air shower size Ne(UL) at Yangbajing level.

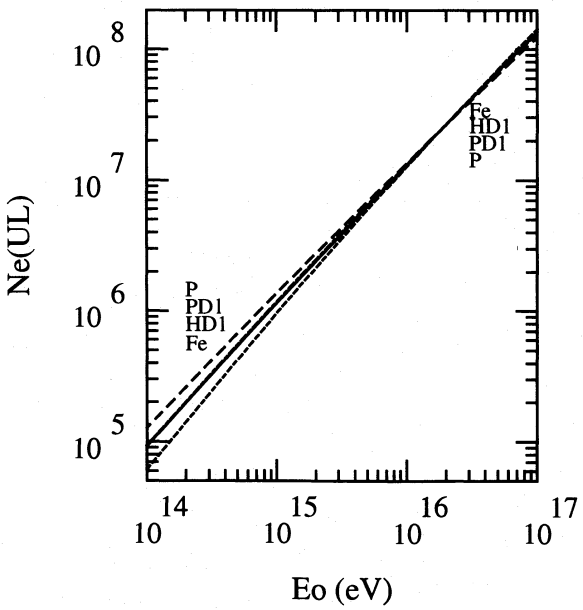

FIG. 5.—Relations between the primary energy E_0 and the average air shower size Ne(UL) for respective primary models. The dashed, chain, solid and dotted lines correspond to the P, PD1, HD1, and Fe models, respectively. Notice that the chain and solid lines almost overlap each other.

cases clearly deviate from those above in the lower energy region and give upper and lower bounds of air shower sizes for the same primary energy, respectively. This is easily understood from the fact that air showers induced by iron primaries develop faster than those by proton primaries, as shown in Figure 2. A numerican relation between the primary energy E_0 and the size Ne(UL) is summarized for each model in Table 2. These approximate relations are valid in the energy region ranging from $\sim 10^{14}$ to 10^{17} eV at Yangbajing altitude and can be used for the energy estimation of primary particles.

For each of the selected air showers, we further adjusted the core position by using the equations in the preceding

TABLE 2

RELATION BETWEEN PRIMARY ENERGY AND AIR SHOWER SIZE[a]

Model	C (eV)	N_b	β_1	β_2
P.....	3.05×10^{15}	4.48×10^6	0.96	1.05
PD1	3.34×10^{15}	4.62×10^6	0.90	1.01
HD1.....	3.67×10^{15}	4.86×10^6	0.91	0.99
Fe	3.90×10^{15}	5.07×10^6	0.83	0.97

[a] The relation between the primary energy E_0 (eV) and air shower size Ne(UL),

$$E_0 = C\left[\frac{Ne(\mathrm{UL})}{Nb}\right]^{\beta_1}\left[1+\frac{Ne(\mathrm{UL})}{Nb}\right]^{\beta_2-\beta_1},$$

is given for each primary model at Yangbajing altitude.

section with the weight parameter $\alpha = 1.8$. Using the Monte Carlo data, we estimated the error of this core location method to be $\Delta r = +5 \pm 2$ m [and Δx (Δy) $= \pm 0 \pm 4$ m]. The first term is a systematic error, and the second one is 1 standard deviation of the distribution.

We determined each air shower size Ne(UL) by fitting the lateral distribution function $F(x, s)$ to the data with a least-squares method. The correct size of each shower is also given by the Monte Carlo simulation. A justification of the size estimation can be examined by comparing it with the Monte Carlo result; the correlation between them is shown in Figure 6. The given size values and the estimated ones are in good agreement. From this Monte Carlo result, we can estimate our systematic uncertainties for the energy determination to be no more than 20% at energies around 10^{15} eV.

We further examined how well our method can reproduce the primary spectrum, using the Monte Carlo showers. Shown in Figure 7. is a comparison between the estimated spectrum, obtained through the procedure mentioned above, and the sampled (or assumed) one in the case of model HD1. Good agreement is seen in the energy region above, $\sim 3 \times 10^{14}$ eV, where the trigger efficiencies of air

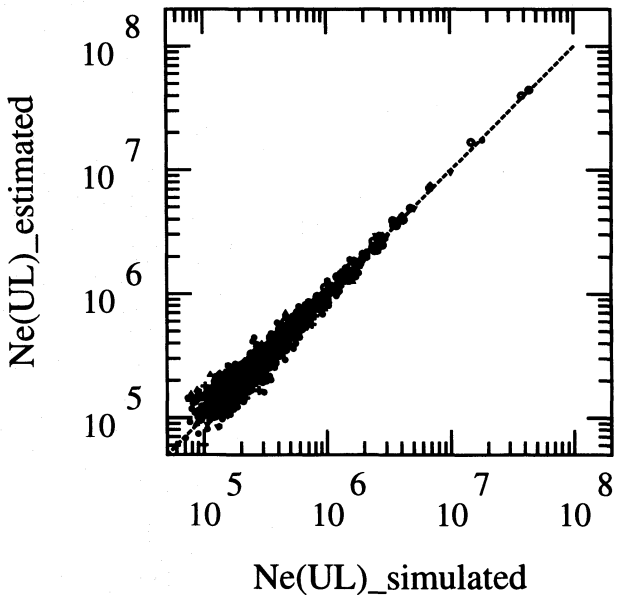

FIG. 6.—Scatter plots of the simulatated Ne(UL) and the estimated Ne(UL) for the Monte Carlo showers.

© American Astronomical Society • Provided by the NASA Astrophysics Data System

1996ApJ...461..408A

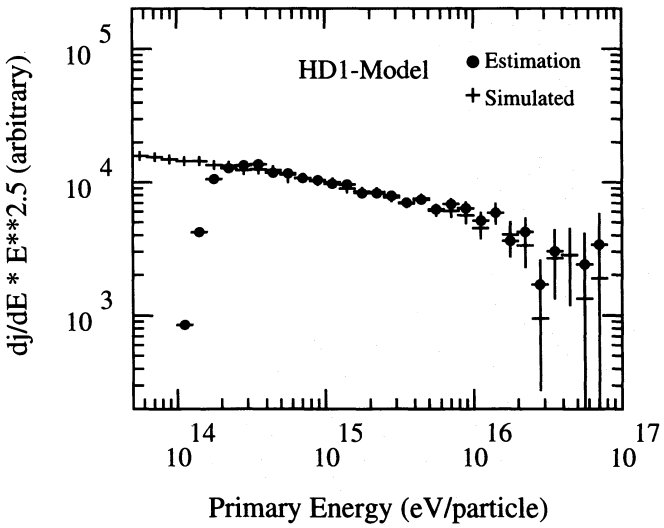

FIG. 7.—Sampled and estimated energy spectra of primary cosmic rays in the case of the HD1 model.

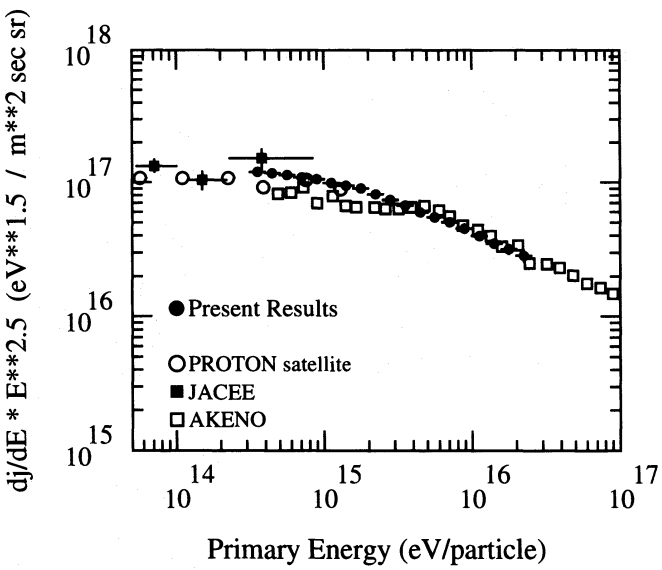

FIG. 8.—Energy spectrum of primary cosmic rays around the knee. Our data are compared with other data from the proton satellite (Grigorov et al. 1971), the JACEE Collaboration (Burnett et al. 1993) and Akeno (Nagano et al. 1984).

showers are ~100% for all primary particles. Such reproducibility is also confirmed for all other models.

On the basis of all the discussions above, we conclude that the energy spectrum of primary cosmic rays around the knee can be obtained with sufficient accuracy using the high-energy air shower data selected as stated in the preceding section.

5. RESULT AND SUMMARY

We analyzed the experimental data obtained with the Tibet array according to the procedure discussed above and obtained the energy spectrum of the primary cosmic rays in the energy range between 3×10^{14} and 2×10^{16} eV. This primary energy bound is determined by taking into account the following. That is, air shower detection under the selection conditions described in § 4.1 rapidly worsens in the energy region less than $\sim 10^{14}$ eV, as seen in Figure 3. On the other hand, when the primary energies exceed several times 10^{16} eV, air shower particles extend far beyond the detector area. Thus the energy estimation error becomes large there and statistics become poor.

Figure 8 shows the differential energy spectrum of total cosmic rays observed with the Tibet air shower array, using a conversion formula in the case of the HD1 model. Our data are also compared with other experiments in the same figure (Grigorov et al. 1971; Nagano et al. 1984; Burnett et al. 1993). The overall primary energy spectrum obtained does not resemble a single power law and shows a gradual steepening of the slope at energies around $E_b = 10^{15.25}$ eV. The spectrum can be expressed as

$$J(E_0) = 1.5 \times 10^{-20}(E_0/10^{14.75}\ \text{eV})^{-2.60\pm0.04} \times (\text{m}^{-2}\ \text{s}^{-1}\ \text{sr}^{-1}\ \text{eV}^{-1}) \text{ at } E_0 < 10^{14.75}\ \text{eV}$$

and

$$J(E_0) = 1.2 \times 10^{-23}(E_0/10^{15.85}\ \text{eV})^{-3.00\pm0.05} \times (\text{m}^{-2}\ \text{s}^{-1}\ \text{sr}^{-1}\ \text{eV}^{-1}) \text{ at } E_0 > 10^{15.85}\ \text{eV},$$

where this changes gradually between $10^{14.75}$ and $10^{15.85}$ eV and takes the value $J(E_0) = 6.7 \times 10^{-22}$ (m^{-2} s^{-1} sr^{-1} eV^{-1}) at $E_0 = 10^{15.25}$ eV.

Our spectrum seems to be smoothly connected to the direct measurements by Grigorov et al. (1971) and the JACEE Collaboration (Burnett et al. 1993) at the lower energy region. The flux values around 10^{15} eV are higher than the Akeno data (Nagano et al. 1984), while those at energies around 10^{16} eV are about 10% lower than theirs. The bending of the spectrum is not as abrupt as the Akeno, and its energy (E_b) is also lower than theirs. Their lower flux at energies around 10^{15} eV could be attributed to very low detection efficiencies of air showers at the Akeno altitude, as discussed in § 3.

If we use the PD1 model for this analysis, however, the flux value decreases by about 10% at energies around 10^{15} eV compared with the HD1 model, while this difference becomes smaller with increasing primary energy. Thus, our spectrum obtained around the knee is almost independent of the primary-mass composition.

The gradual steepening of the spectrum at lower energy may be in favor of shock acceleration at SNRs, which suggests a considerable change in the relative abundance of the various cosmic-ray nuclei as the energy increases, but its confirmation requires more direct information about the primary-mass composition at energies around the knee.

The present air shower array was enlarged by a factor of 4 in 1995 with its effective detection area becoming about seven times as large as the present one. Using this new array, the spectrum can be easily extended up to 10^{17} eV or more with sufficient statistics. This array will also be combined with an emulsion chamber to study the proton component in the knee energy region (Saito et al. 1993). The result then provides important information necessary for understanding the origin and acceleration mechanism of high-energy cosmic rays in our Galaxy.

This work is supported in part by Grants-in-Aid for Scientific Research and also for International Scientific Research from the Ministry of Education, Science, and Culture, in Japan, and by the Committee of National Nature Science Foundation in China.

© American Astronomical Society • Provided by the NASA Astrophysics Data System

1996ApJ...461..408A

REFERENCES

Amenomori, M., et al. 1990, Nucl. Instrum. Methods Phys. Res., A, 288, 619
———. 1992, Phys. Rev. Lett., 69, 2468
———. 1993a, Phys. Rev. D, 47, 2675
———. 1993b, ApJ, 415, L147
———. 1994, ApJ, 429, 634
Axford, W. I. 1991, in Proc. Int. Symp. on Astophysical Aspects of the Most Energetic Cosmic Rays, ed. M. Nagano & F. Takahara (Singapore: World Scientific), 406
———. 1994, ApJS, 90, 937
Bird, D. J., et al. 1993, Phys. Rev. Lett., 71, 340
Bird, D. J., et al. 1994, ApJ, 424, 491
Bradt, H., et al. 1965, Proc. Ninth Int. Cosmic Ray Conf. (London), 2, 715
Burnett, T. H., et al. 1993, Proc. 23d Int. Cosmic Ray Conf. (Calgary), 2, 5
Fitchel, C. E., & Linsley, J. 1986, ApJ, 300, 474
Grigorov, N. L., et al. 1971, Proc. 12th Int. Cosmic Ray Conf. (Hobart), 5, 1746
Hillas, A. M. 1981, Proc. 17th Int. Cosmic Ray Conf. (Paris), 13, 69
———. 1984, ARA&A, 22, 425
Jones, F. C., & Ellison, D. C. 1991, Space Sci. Rev., 58, 259
Kasahara, K., & Torii, S. 1991, Comput. Phys. Commun., 64, 109
Kasahara, K., Yuda, T., & Torii, S. 1990, Proc. 21st Int. Cosmic Ray Conf. (Adelaide), 9, 9
Lagage, P. O., & Cesarsky, C. J. 1983, A&A, 118, 223
Lloyd-Evans, J. 1992, Proc. 22d Int. Cosmic Ray Conf. (Dublin), 5, 215
Nagano, M., et al. 1984, J. Phys. G, 10, 1295
Naito, T., & Takahara, F. 1995, MNRAS, 275, 1077
Peters, B. 1959, Nuovo Cimento (Suppl.), 14, 436
Protheroe, R. J., & Szabo, A. P. 1992, Phys. Rev. Lett., 69, 2885
Ren, J. R., et al. 1988, Phys. Rev. D, 38, 1404
Saito, To., et al. 1993, Astropart. Phys., 1, 257
Yoshida, S., et al. 1995, Astropart. Phys., 3, 105

© American Astronomical Society • Provided by the NASA Astrophysics Data System